

Direct Measurement of the $^{59}\text{Cu}(p, \alpha)^{56}\text{Ni}$ Excitation Function to Constrain the Ni–Cu Cycle Strength and Its Impact on Explosive Nucleosynthesis

E. Lopez-Saavedra , ^{1,*} M. L. Avila , W.-J. Ong , P. Mohr , S. Ahn , H. Arora , L. Balliet , K. Bhatt , S.M. Cha , K. A. Chipps , J. Dopfer , I. A. Tolstukhin , R. Jain , M.J. Kim , K. Kolos , F. Montes , D. Neto , S. D. Pain , J. Pereira , J. S. Randhawa , L. J. Sun , C. Ugalde , and L. Wagner

¹Physics Division, Argonne National Laboratory, Lemont, Illinois 60439, USA

²Nuclear and Chemical Sciences Division, Lawrence Livermore National Laboratory, Livermore, California 94550, USA

³HUN-REN Institute for Nuclear Research (ATOMKI), H-4001 Debrecen, Hungary

⁴Center for Exotic Nuclear Studies, Institute for Basic Science, Daejeon 34126, Republic of Korea

⁵Facility for Rare Isotope Beams (FRIB), Michigan State University, East Lansing, MI 48824, USA

⁶University of Notre Dame, Dept. of Physics and Astronomy, Notre Dame, IN 46556, USA

⁷Oak Ridge National Laboratory, Tennessee, USA

⁸Extreme Rare Isotope Science, Institute for Rare Isotope Science (IRIS),

¹Gukjegwahak-ro, Yuseong-gu, Daejeon 34000, Republic of Korea

⁹Department of Physics, University of Illinois Chicago, 845 W. Taylor St., Chicago, IL 60607, USA

¹⁰Department of Physics and Astronomy, Mississippi State University, Mississippi State, MS 39762, USA

(Dated: 2nd February 2026)

A new direct measurement of the $^{59}\text{Cu}(p, \alpha)^{56}\text{Ni}$ excitation function from 2.43–5.88 MeV in the center-of-mass was performed in inverse kinematics using the high-efficiency MUSIC active-target detector at FRIB. This reaction plays a critical role in constraining the strength of the Ni–Cu cycle in different explosive astrophysical scenarios such as Type I X-ray bursts and the νp -process in neutrino-driven winds after a core-collapse supernova. The newly derived stellar rate is systematically lower than REACLIB, leading to less than 0.1% recycling through the Ni–Cu cycle in X-ray bursts and to an enhanced efficiency for the νp -process up to $T_9 \approx 3.7$.

Explosive nucleosynthesis in proton-rich environments occurs in several astrophysical scenarios, including Type I X-ray bursts (XRBs) on accreting neutron stars, where the rp -process [1, 2] operates, and in proton-rich ($Y_e > 0.5$) neutrino-driven winds following core-collapse supernovae (CCSNe), where the νp -process takes place [3–5]. Understanding these astrophysical environments requires a comprehensive, interdisciplinary approach. Crucially, it demands detailed knowledge of nuclear physics, including reaction rates, nuclear structure, and decay properties [6–9]. In both scenarios, the production of proton-rich nuclei proceeds through extended sequences of proton captures on unstable isotopes, but while the rp -process is dominated by (p, γ) reactions and subsequent β^+ decays, the νp -process relies on a combination of (p, γ) and (n, p) reactions.

Type I XRBs are the most common thermonuclear explosions in the Galaxy and serve as powerful laboratories for studying the physics of neutron stars, which are the densest visible form of matter in the Universe [2, 3, 10, 11]. Because XRB light curves and ashes contain information about neutron-star structure and explosive nucleosynthesis, detailed modeling of these events is essential for interpreting observations and connecting them to underlying physics [12, 13]. XRB simulations rely on large reaction networks involving hundreds of short-lived nuclei with poorly constrained reaction rates. These uncertainties produce strong model sensitivities that directly influence the predicted burst energy genera-

tion, light curve and the resulting ashes composition [14].

In the case of the νp -process, antineutrino captures on free protons generate neutrons that, through (n, p) reactions, allow the reaction flow to bypass β -decay waiting points and proceed beyond the Fe group. The νp -process may thereby contribute to the synthesis of the light p nuclei, the neutron-deficient stable isotopes above iron that cannot be produced by the classical s - and r -processes [15].

A particularly important branching point during nucleosynthesis on both processes arises in the mass region around ^{59}Cu , where the competition between the $^{59}\text{Cu}(p, \alpha)^{56}\text{Ni}$ and $^{59}\text{Cu}(p, \gamma)^{60}\text{Zn}$ reactions defines the Ni–Cu cycle and sets the conditions under which the reaction flow can proceed toward heavier nuclei. If the (p, α) channel dominates, material is driven back to the Ni region, confining nucleosynthesis and limiting the production of heavier nuclei, whereas a stronger (p, γ) channel allows the reaction flow to escape the Ni–Cu cycle and advance toward higher- Z nuclei [16, 17]. As a result, the temperature dependence and relative strengths of these two reactions play a central role in shaping nucleosynthesis in both the rp and νp processes.

In XRBs, recent sensitivity studies [14, 18, 19] identified that the $^{59}\text{Cu}(p, \alpha)^{56}\text{Ni}$ reaction strongly affects energy generation and nucleosynthesis, particularly near the waiting-points ^{56}Ni and ^{60}Zn [20].

In the νp -process, if the cross-over temperature at which the (p, γ) rate on ^{59}Cu overtakes the (p, α) rate

were shifted to slightly higher values (i.e., $T_9 > 3$), the reaction flow would begin moving toward heavier nuclei closer to the proto-neutron-star surface, where the neutrino flux is substantially stronger. This would enhance the efficiency of the νp -process by increasing the rate of (n, p) reactions that bypass β -decay waiting points [5].

Therefore, improved constraints on the $^{59}\text{Cu}(p, \alpha)^{56}\text{Ni}$ and $^{59}\text{Cu}(p, \gamma)^{60}\text{Zn}$ reaction rates, and on their branching ratio, are essential for reliably predicting breakout from the Ni–Cu cycle and the resulting rp -process in XRBs and the νp -process in neutrino-driven proton-rich winds after CCSN.

The first direct measurement of the $^{59}\text{Cu}(p, \alpha)$ reaction was performed by Randhawa *et al.* [21], who reported a single data point at $E_{\text{cm}} = 6.0 \pm 0.3$ MeV. Their measured cross section was found to be a factor of ~ 1.6 –4 lower than statistical-model predictions, suggesting a suppressed (p, α) strength. Two additional data points between 4 and 5 MeV have very recently become available [22]. Other attempts to constrain this reaction have relied on spectroscopic information of states in ^{60}Zn [16, 23]. However, the resulting constraints suffer from significant uncertainties, primarily due to the lack of experimental data on the corresponding α -particle partial widths. These previous studies highlighted the need for more comprehensive measurements of the (p, α) reaction to properly assess the strength of the Ni–Cu cycle. A series of experiments is planned and ongoing to study the Ni–Cu cycle; a comprehensive overview was provided recently in Ref. [24].

In this work, a new direct measurement of the $^{59}\text{Cu}(p, \alpha)^{56}\text{Ni}$ excitation function, extending down to $E_{\text{cm}} = 2.43$ MeV, is presented, providing the strongest constraints to date on the astrophysical reaction rate. This significantly reduces the uncertainties for this key reaction in the Ni–Cu cycle and enables a more accurate assessment of its impact on nucleosynthesis in XRBs and the νp -process in CCSN.

The experiment was performed in inverse kinematics at the Facility for Rare Isotope Beams (FRIB) using the Multi-Sampling Ionization Chamber (MUSIC) detector [25]. The 8.418 MeV/u ^{59}Cu beam was obtained in-flight by fragmentation of the 240 MeV/u ^{64}Zn primary beam and sent to the ReA6 beamline. The ^{59}Cu beam delivered to MUSIC had an average purity of approximately 94% and an intensity of $\sim 9 \times 10^3$ particles per second (pps). MUSIC was filled with methane gas at 440 Torr, which completely stopped the beam inside of the detector. The only beam contaminant was ^{59}Ni , contributing approximately 6% of the total beam.

The MUSIC detector is an active-target system with an anode segmented into 18 strips, where the middle 16 strips are further divided into left and right sections, as described in Ref. [25]. This enables measurement of the energy loss of different particles along the detector as they traverse the gas, allowing particle identification.

When a (p, α) reaction occurs at any anode strip, the heavy recoil ^{56}Ni can be distinguished because it exhibits a lower energy loss than the unreacted ^{59}Cu beam. By summing the energy deposited in consecutive strips after the reaction point, a ΔE – ΔE analysis can be performed to further separate the different reaction channels [26].

From the experimental data, cross sections for 8 strips were extracted corresponding to effective energies in the center-of-mass frame between 2.43 MeV and 5.88 MeV, as shown in Table I. Effective center-of-mass energies, $E_{\text{c.m.}}^{\text{eff}}$, were calculated by first deducing the center-of-mass energies from the measured beam energy losses in the MUSIC detector and then applying corrections for thick-target yield effects [27]. The uncertainty in the center-of-mass energy arises from the uncertainty in the beam energy (0.5% FWHM) and the uncertainty in the beam's energy loss in different strips of the detector (5%) (see Ref. [26] for details). The estimated total energy loss of the beam in each anode strip defines the center-of-mass energy binning, ΔE_{cm} . The systematic uncertainty of the cross sections originates primarily from the analysis methods and the different criteria used to select the events of interest.

Table I: Measured effective energies and cross sections with statistical and systematic uncertainties.

$E_{\text{cm}}^{\text{eff}}$ (MeV)	ΔE_{cm} (MeV)	σ (mb)	$\Delta\sigma_{\text{stat}}$ (mb)	$\Delta\sigma_{\text{sys}}$ (mb)
5.88 (3)	+0.18 -0.26	7.024	0.220	2.355
5.44 (3)	+0.18 -0.27	3.412	0.154	0.612
4.98 (4)	+0.19 -0.28	1.861	0.113	0.300
4.49 (4)	+0.21 -0.28	0.619	0.065	0.092
4.02 (4)	+0.19 -0.31	0.248	0.042	0.083
3.54 (4)	+0.17 -0.37	0.082	0.024	0.014
2.98 (5)	+0.19 -0.37	<0.015	—	—
2.43 (5)	+0.18 -0.42	<0.011	—	—

Statistical uncertainties for the first strips were determined assuming Poisson statistics. For very low-statistics strips, confidence intervals were estimated using the Feldman–Cousins approach [28]. For Strips 8 and 9, the last two data points in Table I, with 2 and 1 events, respectively, and an assumed background of 5 counts, have 95% C.L. intervals of [0.00, 2.49] and [0.00, 1.88].

Fig. 1 compares the measured cross sections with available experimental data [21, 22], the NON-SMOKER predictions scaled by a factor of 0.49, as well as with TALYS [29] calculations employing the Demetriou and Gordeyev dispersive α -optical model potential (α –OMP) [30], which best reproduces the experimental data. To achieve quantitative agreement, the calculated TALYS cross sections were scaled by a factor of 0.86, corresponding to the value that minimizes the reduced chi-square, between the theoretical prediction and the experimental excitation function. At the energy closest to the Randhawa *et al.* data point ($E_{\text{cm}} \approx 6.0 \pm 0.3$ MeV), our measurement

at $E_{\text{cm}} = 5.88$ MeV yields a cross section roughly a factor of 1.5 higher, yet still consistent within the quoted uncertainties. Ref. [22] reported two alternative extractions of the angle-integrated cross section from the same data-set, based on TALYS-derived and Legendre-fit angular distributions; the large separation between these results illustrates a strong sensitivity to the angular-integration method, indicating that the angle-integrated cross sections are not robustly constrained by the available angular information. An important observation from Fig. 1 is that the NON-SMOKER calculations scaled by a factor of 0.49, as adopted by Bhathi et al., do not reproduce the energy dependence observed in our data.

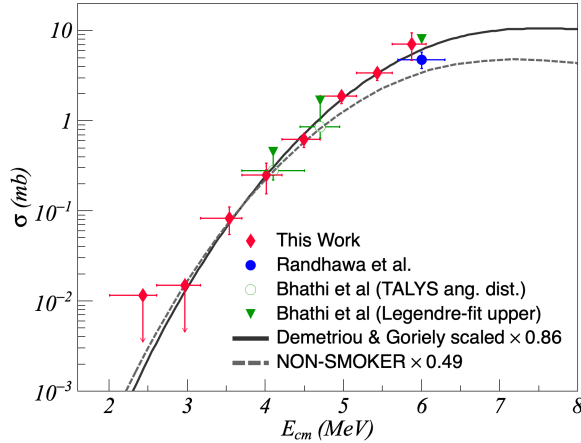


Figure 1: Measured $^{59}\text{Cu}(p, \alpha)^{56}\text{Ni}$ cross sections from the present work, Randhawa *et al.* [21], and Bhathi *et al.* [22], compared with the NON-SMOKER predictions scaled by 0.49 (gray dotted line) and TALYS calculations scaled by 0.86 using the Demetriou and Goriely dispersive α -OMP [30] (black line).

The present work provides an experimentally constrained reaction rate in the $T_9 \sim 2.6\text{--}10.5$ temperature range, including our upper-limit cross-section values. This temperature coverage was determined numerically by evaluating the effective energy window contributing to the stellar rate following the formalism of Ref. [31]. In XRBs, reaction rates are relevant down to $T_9 \lesssim 1$, while for the νp -process in CCSN, they span $T_9 \simeq 1\text{--}3$. To extend the rate toward lower temperatures, the experimental (p, α) cross sections were combined with calculations using the statistical model and the TALYS code.

In a slightly oversimplified notation, the cross section of (p, α) reactions scale as

$$\sigma_{(p, \alpha)} \propto \frac{T_{p0} T_\alpha}{T_p + T_\gamma + T_\alpha} \approx \frac{T_{p0} T_{\alpha0}}{T_p} \quad (1)$$

where the approximation holds for the energies under study. The T_i are the transmissions to the open channels, summed over all states j in the residual nuclei: $T_i =$

$\sum_j T_{i,j}$. T_{p0} is the transmission in the entrance channel (with the target ^{59}Cu in its ground state); $T_\alpha \approx T_{\alpha0}$ is dominated by the transition to the ^{56}Ni ground state; excited states are suppressed because of the lower α energy for the population of excited states in the doubly-magic ^{56}Ni nucleus.

Eq. (1) indicates that the calculated (p, α) cross section depends on the proton optical model potential (pOMP) (via T_p and T_{p0}), the α -OMP via $T_{\alpha0}$, and the level density (LD) in ^{59}Cu via T_p . For further information on the role of the transmissions T_i , see [32]. The role of the pOMP remains minor because changes in the proton transmission affect T_{p0} and T_p in a similar way, leading to an almost unchanged ratio T_{p0}/T_p in Eq. (1).

Thus, to identify the optimal TALYS settings for extrapolating the reaction rate, one has to focus on the α -OMP and the LD. As already noted in [21], all α -OMPs tend to overestimate the experimental (p, α) cross section, a trend confirmed in the present work. Consequently, we use the Demetriou *et al.* dispersive α -OMP, which gives the lowest (p, α) cross section. A consistent performance of this potential was also reported by Gyürky *et al.* for the $^{64}\text{Zn}(p, \alpha)^{61}\text{Cu}$ reaction [33], where TALYS calculations using the same Demetriou potential reproduced the experimental data well. An alternative approach [34], in which the pOMP was modified, leads to a somewhat flatter energy dependence, which will be discussed further in [26]. The treatment of the LD in ^{59}Cu was varied, and a χ^2 -based best fit was obtained for the Skyrme-Hartree-Fock-Bogolyubov model [35]. To further optimize the agreement with the data, the corresponding TALYS prediction was uniformly scaled, and a reduction factor of 0.86 provided the lowest reduced χ^2 (see Fig. 1).

The excellent agreement between the experimental data and the optimized TALYS calculation indicates that the LD in the compound nucleus ^{60}Zn is sufficiently high for the application of the statistical model. However, Ref. [36] noted that the LD in ^{60}Zn may behave unusually around excitation energies of 5–6 MeV, corresponding to proton energies below 1 MeV, which are relevant for the relatively low temperatures in XRBs. This feature raises concerns about the applicability of the statistical model for reaction-rate calculations at low temperatures ($T_9 \lesssim 1$). As this potential systematic uncertainty is difficult to quantify, in this work an uncertainty factor of 1.5 was adopted for the statistical-model calculations, under the assumption that the statistical model remains applicable also in the lower-energy regime. Typically, this assumption holds down to about $T_9 \approx 1$ even for lighter nuclei [37].

Our measurement constrains only the ground-state contribution of ^{59}Cu to the stellar rate. This reaction rate was obtained using an Exp2Rate [38] calculation that combines the experimental data with the TALYS-predicted cross sections scaled to the measurement. The

stellar rate, which includes contributions from thermally populated excited states in ^{59}Cu , was calculated with TALYS and scaled by the same factor of 0.86 used for the ground state.

To assess the reliability of the stellar rate, the ground-state contribution $X(T_9)$ was calculated using the expression

$$X(T) = \frac{1}{f_{\text{SEF}}(T) G_0(T)} \quad (2)$$

which defines the maximum reduction in the reaction-rate uncertainty that can be achieved through a laboratory measurement [39]. Here, $f_{\text{SEF}}(T)$ is the stellar enhancement factor and $G_0(T)$ is the nuclear partition function normalized to the ground state. The stellar enhancement factor $f_{\text{SEF}}(T)$ was extracted by calculating the ratio of the stellar rate to the ground-state rate derived in this work. Using the same TALYS setup, the temperature-dependent partition function $G_0(T)$ was obtained. The uncertainty on $f_{\text{SEF}}(T)$ was determined by varying both the level-density models and the number of thermally populated states included in the calculation, and propagated into the final stellar-rate uncertainty.

In the temperature range covered by our measurement, $2.6 \leq T_9 \leq 10.5$, the ground-state contribution decreases from $X \simeq 0.75$ at $T_9 \approx 2.6$ to $X \simeq 0.10$ at $T_9 \approx 10$. This implies that our experiment directly constrains about three quarters of the stellar reaction rate at $T_9 \approx 2.6$, while the remaining contribution originates from reactions on thermally populated excited states and therefore remains model dependent.

Fig. 2 presents the recommended stellar $^{59}\text{Cu}(p, \alpha)^{56}\text{Ni}$ reaction rate from this work together with the currently adopted REACLIB rate based on NON-SMOKER calculations [40] over the temperature range $T_9 = 0.1-10$. The tabulated stellar reaction rate with upper and lower uncertainty bounds are provided in Ref. [26]. The REACLIB rates have been widely used in sensitivity studies [12, 14, 18]; therefore, we focus the present discussion on a comparison with REACLIB. A more extended analysis will be provided in Ref. [26].

The bottom panel of Fig. 2 shows the log of the ratio of the stellar $^{59}\text{Cu}(p, \alpha)^{56}\text{Ni}$ reaction rate derived in this work to the REACLIB rate. At low temperatures the new rate is suppressed by more than an order of magnitude relative to REACLIB. The ratio gradually increases with temperature, exceeding unity only above $T_9 \approx 4.55$ mainly due to a visible dip in the REACLIB parametrization, and falls below unity again at $T_9 \gtrsim 9$. Overall, at temperatures relevant to XRBs and the νp -process, the $^{59}\text{Cu}(p, \alpha)^{56}\text{Ni}$ reaction rate obtained in this work is systematically lower than the NON-SMOKER prediction widely used in astrophysical models and also below the recent REACLIB scaled by 0.49, as suggested in Ref. [22], indicating a significantly reduced efficiency of the (p, α) channel.

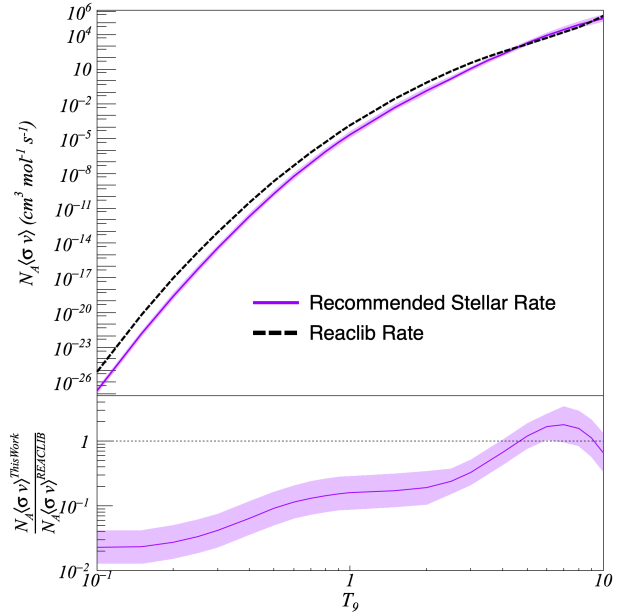


Figure 2: (Top) Recommended $^{59}\text{Cu}(p, \alpha)^{56}\text{Ni}$ stellar reaction rate from the present work (purple line) with propagated uncertainties (shaded band) compared to the REACLIB rate (green line). (Bottom) Ratio of the recommended stellar rate from this work to the REACLIB rate.

To properly assess the impact of the present results on explosive nucleosynthesis in XRBs and the νp -process, it is critical to determine the competition between the (p, α) and (p, γ) channels. For this comparison, the theoretical $^{59}\text{Cu}(p, \gamma)^{60}\text{Zn}$ REACLIB rate was used. A recent experimental study by O’Shea *et al.* [23], who used the $^{59}\text{Cu}(d, n)^{60}\text{Zn}$ reaction to study the proton-unbound resonant states in ^{60}Zn , obtained a (p, γ) rate that is in good agreement with the REACLIB rate over the temperature range of interest.

The cycle strength can be quantified by the reaction rate branching ratio [41]. Values of $B_{p\alpha/p\gamma} > 1$ correspond to a strong Ni–Cu cycle [16] where the reaction flow predominantly cycles back to lower masses, whereas $B_{p\alpha/p\gamma} < 1$ indicates that (p, γ) breakout dominates and nucleosynthesis proceeds toward heavier nuclei. Fig. 3 shows the branching ratio $B_{p\alpha/p\gamma}$ derived from the recommended (p, α) rate with its associated uncertainties, and the mean value of the REACLIB (p, γ) rate. For comparison, the figure also shows $B_{p\alpha/p\gamma}$ calculated using the REACLIB (p, α) rate with an uncertainty of a factor of 100 up and down and the mean value of the REACLIB (p, γ) rate.

Previous sensitivity studies typically varied the relevant reaction rates such that the branching ratio reached unity at temperatures $T_9 \lesssim 2$ to artificially enforce a strong Ni–Cu cycle and probe its potential impact on the burst light curve and ash composition. For ex-

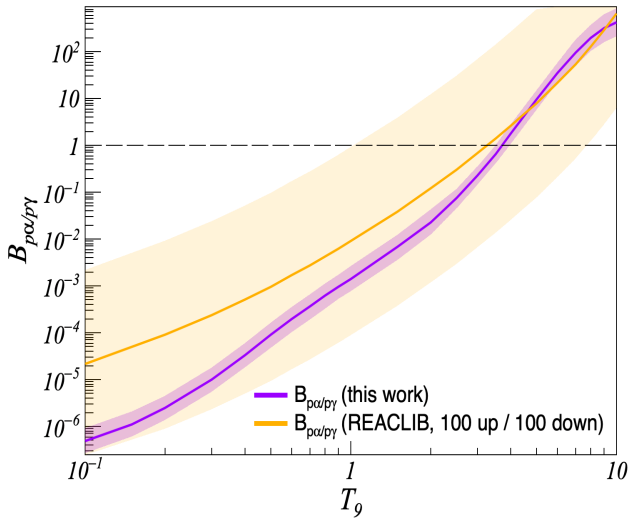


Figure 3: Branching ratio of the $^{59}\text{Cu}(p, \alpha)^{56}\text{Ni}$ to $^{59}\text{Cu}(p, \gamma)^{60}\text{Zn}$ stellar reaction rates as a function of temperature. The purple curve and shaded band show the recommended ratio and its uncertainty based on the experimentally constrained (p, α) rate. The green curve and band illustrate the REACLIB rate varied by ± 100

ample, Parikh *et al.* [12] found that increasing the NON-SMOKER rates by a factor of 10 strengthened the Ni–Cu cycle. Cyburt *et al.* [14] and Meisel *et al.* [18] varied the REACLIB rates by a factor of 100, likewise producing a stronger cycle.

Using the experimentally constrained (p, α) rate, the uncertainty on the branching ratio is significantly reduced, allowing the cycle behavior to be constrained with much higher precision. Our results show that in the range of temperatures relevant for XRBs ($T_9 \lesssim 1$), the branching ratio remains extremely small, $B_{p\alpha/p\gamma} \lesssim 10^{-3}$, indicating that the (p, γ) channel dominates by several orders of magnitude. Consequently, recycling through the Ni–Cu cycle in this temperature range is negligible (at the level of $\lesssim 0.1\%$) and the reaction flow continues directly toward heavier nuclei. For νp -process conditions, where typical temperatures lie around $T_9 \approx 1\text{--}3$, we obtain $B_{p\alpha/p\gamma} \approx 10^{-3}$ at $T_9 = 1$, and ≈ 0.22 at $T_9 = 3$. These values imply that only about 0.1% to $\sim 22\%$ of the flow is recycled through the Ni–Cu cycle in this temperature range, so that the majority of the reaction flux still escapes toward heavier nuclei. Notice how the branching ratio calculated with the rate derived in this work approaches $B_{p\alpha/p\gamma} \sim 1$ at $T_9 \approx 3.7$, whereas the REACLIB rate predicts a lower crossover temperature around $T_9 \approx 3.2$. By placing the crossover at a higher temperature, our results imply that the flow toward heavier nuclei begins closer to the proto–neutron star surface, where the neutrino flux is larger, thereby increasing the overall efficiency of the νp -process, as suggested by Arcones *et*

al. [5].

Thus, our measurement delivers the first tightly constrained determination of the Ni–Cu cycle strength, pinpointing the temperatures at which recycling through ^{56}Ni becomes significant and those where breakout toward heavier nuclei proceeds.

In summary, this work reports a new direct measurement of the $^{59}\text{Cu}(p, \alpha)^{56}\text{Ni}$ excitation function over $E_{\text{cm}} = 2.43\text{--}5.88$ MeV. From these data, a new stellar (p, α) reaction rate was derived that is lower than the REACLIB evaluation. Using this experimentally constrained (p, α) rate, the uncertainty on the branching ratio is significantly reduced, allowing the cycle behavior to be determined with much higher precision. The results show that recycling through the Ni–Cu cycle in X-ray bursts is suppressed to below 0.1%, while the crossover to (p, γ) capture is shifted to $T_9 \approx 3.7$, placing νp -process breakout in a region of higher neutrino flux and enhancing nucleosynthesis toward heavier nuclei.

This work is based upon work supported by the U.S. Department of Energy, Office of Science, Office of Nuclear Physics, under Contract No. DE-AC02-06CH11357 and DE-AC05-00OR22725. It used resources of the Facility for Rare Isotope Beams (FRIB) Operations, which is a DOE Office of Science User Facility under Award Number DE-SC0023633. This work was also supported by the Institute for Basic Science (IBS) funded by the Ministry of Science and ICT, Korea (Grant No. IBS-R031-D1), and by NKFIH (K134197). This work was also performed under the auspices of the U.S. Department of Energy by Lawrence Livermore National Laboratory under contract DE-AC52-07NA27344.

* elopezaavedra@anl.gov

- [1] R. K. Wallace and S. E. Woosley, Explosive hydrogen burning, *Astrophysical Journal Supplement Series* **45**, 389 (1981).
- [2] S. E. Woosley and R. E. Taam, γ -ray bursts from thermonuclear explosions on neutron stars, *Nature* **263**, 101 (1976).
- [3] A. Parikh, J. José, G. Sala, and C. Iliadis, Nucleosynthesis in Type I X-ray Bursts, *Progress in Particle and Nuclear Physics* **69**, 225 (2013).
- [4] C. Fröhlich, G. Martínez-Pinedo, M. Liebendörfer, F.-K. Thielemann, E. Bravo, W. R. Hix, K. Langanke, and N. T. Zinner, Neutrino-induced nucleosynthesis of $A > 64$ nuclei: The νp process, *Phys. Rev. Lett.* **96**, 142502 (2006).
- [5] A. Arcones, C. Fröhlich, and G. Martínez-Pinedo, Impact of supernova dynamics on the νp -process, *The Astrophysical Journal* **750**, 18 (2012).
- [6] F.-K. Thielemann, C. Fröhlich, R. Hirschi, M. Liebendörfer, I. Dillmann, D. Mocelj, T. Rauscher, G. Martínez-Pinedo, K. Langanke, K. Farouqi, K.-L. Kratz, B. Pfeiffer, I. Panov, D. K. Nadyozhin, S. Blin-

nikov, E. Bravo, W. R. Hix, P. Höflich, and N. T. Zinner, Production of intermediate-mass and heavy nuclei, *Progress in Particle and Nuclear Physics* **59**, 74 (2007), international Workshop on Nuclear Physics 28th Course.

[7] F.-K. Thielemann, I. Dillmann, K. Farouqi, T. Fischer, C. Fröhlich, A. Kelic-Heil, I. Korneev, K.-L. Kratz, K. Langanke, and M. Liebendörfer, The r-, p-, and ν p-process, in *Journal of Physics: Conference Series*, Nuclear Physics in Astrophysics IV, 8–12 June 2009, Laboratori Nazionali di Frascati, Frascati, Italy, Vol. 202 (IOP Publishing, 2010) p. 012006.

[8] F. Käppeler, F.-K. Thielemann, and M. Wiescher, CURRENT QUESTS IN NUCLEAR ASTROPHYSICS AND EXPERIMENTAL APPROACHES, *Annual Review of Nuclear and Particle Science* **48**, 175 (1998).

[9] K. Langanke, F.-K. Thielemann, and M. Wiescher, Nuclear Astrophysics and Nuclei Far from Stability, in *The Euroschool Lectures on Physics with Exotic Beams*, Vol. I, Lecture Notes in Physics, Vol. 651, edited by M. Beyer, Y. Blumenfeld, and M. Dörr (Springer-Verlag, Berlin Heidelberg, 2004) pp. 383–467.

[10] T. M. Belloni, M. Méndez, and C. Zhang, eds., *Timing Neutron Stars* (Springer, Berlin, Heidelberg, 2021).

[11] N. Degenaar and V. F. Suleimanov, Testing the equation of state with electromagnetic observations, in *The Physics and Astrophysics of Neutron Stars*, edited by L. Rezzolla, P. Pizzochero, D. I. Jones, N. Rea, and I. Vidaña (Springer International Publishing, Cham, 2018) pp. 185–253.

[12] A. Parikh, J. José, F. Moreno, and C. Iliadis, The effects of variations in nuclear processes on type i x-ray burst nucleosynthesis, *The Astrophysical Journal Supplement Series* **178**, 110 (2008).

[13] A. W. Steiner, J. M. Lattimer, and E. F. Brown, The equation of state from observed masses and radii of neutron stars, *The Astrophysical Journal* **722**, 33 (2010).

[14] R. H. Cyburt, A. M. Amthor, A. Heger, E. Johnson, L. Keek, Z. Meisel, H. Schatz, and K. Smith, Dependence of x-ray burst models on nuclear reaction rates, *The Astrophysical Journal* **830**, 55 (2016).

[15] C. Fröhlich, The vp-process: critical nuclear physics and astrophysical implications, *Journal of Physics: Conference Series* **403**, 012034 (2012).

[16] C. Kim, K. Chae, S. Cha, K. Kwak, G. Seong, and M. Smith, Estimation of the nicu cycle strength and its impact on Type I X-ray Bursts, *The Astrophysical Journal* **929**, 96 (2022).

[17] Y. H. Lam, N. Lu, A. Heger, A. M. Jacobs, N. A. Smirnova, T. K. Nieto, Z. Johnston, and S. Kubono, The regulated nicu cycles with the new $^{57}\text{Cu}(p,\gamma)^{58}\text{Zn}$ reaction rate and its influence on Type I X-ray bursts: the gs 1826–24 clocked burster, *The Astrophysical Journal* **929**, 73 (2022).

[18] Z. Meisel, G. Merz, and S. Medvid, Influence of nuclear reaction rate uncertainties on neutron star properties extracted from x-ray burst model-observation comparisons, *The Astrophysical Journal* **872**, 84 (2019).

[19] I. Sultana, A. Estradé, B. S. Meyer, and H. Schatz, Sensitivity of nuclear reaction rates in x-ray burst models, arXiv e-prints [10.48550/arXiv.2510.15441](https://arxiv.org/abs/10.48550/arXiv.2510.15441) (2025), draft version October 20, 2025, arXiv:2510.15441 [astro-ph.HE].

[20] L. van Wormer, J. Görres, C. Iliadis, M. Wiescher, and F.-K. Thielemann, Reaction rates and reaction sequences in the rp -process, *Astrophys. J.* **432**, 326 (1994).

[21] J. S. Randhawa, R. Kanungo, J. Refsgaard, P. Mohr, et al., First direct measurement of $^{59}\text{Cu}(p,\alpha)^{56}\text{Ni}$: A step towards constraining the ni–cu cycle in the cosmos, *Phys. Rev. C* **104**, L042801 (2021).

[22] N. Bhathi, J. S. Randhawa, R. Kanungo, J. Refsgaard, M. Alcorta, T. Ahn, C. Andreoiu, D. Bardayan, S. S. Bhattacharjee, B. Davids, G. Christian, A. A. Chen, R. Coleman, P. E. Garrett, G. F. Grinyer, E. Gyabeng Fuakye, G. Hackman, R. Jain, K. Kapoor, R. Krucken, A. Laffoley, A. Lennarz, J. Liang, Z. Meisel, A. Psaltis, A. Radich, M. Rocchini, J. S. Rojo, N. Saei, M. Saxena, M. Singh, C. E. Svensson, P. Subramaniam, A. Talebitaher, S. Upadhyayula, C. Waterfield, J. Williams, M. Williams, and M. A. Zubair, Direct measurement of $^{59}\text{Cu}(p,\alpha)^{56}\text{Ni}$ precludes a strong Ni–Cu cycle in Type-I x-ray bursts (2025), arXiv:2512.12025 [astro-ph.HE].

[23] C. O’Shea, G. Lotay, A. Gade, et al., Single-nucleon transfer unveils NiCu cycle in astrophysical X-ray Bursts, *Research Square* (2025), Preprint, Version 1.

[24] L. J. Sun, J. Dopfer, A. Adams, C. Wrede, A. Banerjee, B. A. Brown, J. Chen, E. A. M. Jensen, R. Mahajan, T. Rauscher, C. Sumithrarachchi, L. E. Weghorn, D. Weisshaar, and T. Wheeler, Extension of the particle x-ray coincidence technique: The lifetimes and branching ratios apparatus, *Phys. Rev. C* **111**, 055806 (2025).

[25] P. F. F. Carnelli, S. Almaraz-Calderon, K. E. Rehm, et al., Multi-sampling ionization chamber (music) for measurements of fusion reactions with radioactive beams, *Nucl. Instrum. Methods Phys. Res. A* **799**, 197 (2015).

[26] E. Lopez-Saavedra, M. L. Avila, W.-J. Ong, P. Mohr, et al., Detailed study of the $^{59}\text{Cu}(p,\alpha)^{56}\text{Ni}$ reaction and constraints on its astrophysical reaction rate (2025), <https://insert-URL-here>.

[27] C. E. Rolfs and W. S. Rodney, *Cauldrons in the Cosmos: Nuclear Astrophysics* (University of Chicago Press, Chicago, IL, 1987).

[28] G. J. Feldman and R. D. Cousins, Unified approach to the classical statistical analysis of small signals, *Physical Review D* **57**, 3873 (1998).

[29] A. Koning, S. Hilaire, and S. Goriely, Talys: modeling of nuclear reactions, *The European Physical Journal A* **59**, 131 (2023).

[30] P. Demetriou, C. Grama, and S. Goriely, Improved global α -optical model potentials at low energies, *Nuclear Physics A* **707**, 253 (2002).

[31] T. Rauscher, Relevant energy ranges for astrophysical reaction rates, *Phys. Rev. C* **81**, 045807 (2010).

[32] P. Mohr, Z. Fülöp, G. Gyürky, Z. Halász, G. G. Kiss, S. R. Kovács, Z. Mátyus, T. N. Szegedi, and T. Szűcs, The α -nucleus potential: towards a solution of a long-standing problem, *Eur. Phys. J. A* **61**, 89 (2025).

[33] G. Gyürky, Z. Fülöp, Z. Halász, G. G. Kiss, and T. Szűcs, Direct study of the α -nucleus optical potential at astrophysical energies using the $^{64}\text{Zn}(p,\alpha)^{61}\text{Cu}$ reaction, *Phys. Rev. C* **90**, 052801 (2014).

[34] V. Avrigeanu and M. Avrigeanu, Charged-particle optical potentials tested by first direct measurement of the $^{59}\text{Cu}(p,\alpha)^{56}\text{Ni}$ reaction, *Phys. Rev. C* **106**, 024615 (2022).

[35] S. Goriely, F. Tondeur, and J. Pearson, A hartree–fock nuclear mass table, [Atomic Data and Nuclear Data Tables](#) **77**, 311 (2001).

[36] D. Soltesz, M. A. A. Mamun, A. V. Voinov, Z. Meisel, B. A. Brown, C. R. Brune, S. M. Grimes, H. Hadizadeh, M. Hornish, T. N. Massey, J. E. O'Donnell, and W. E. Ormand, Determination of the ^{60}Zn level density from neutron evaporation spectra, [Phys. Rev. C](#) **103**, 015802 (2021).

[37] P. Mohr, Uncertainty of the astrophysical $^{17,18}\text{O}(\alpha, n)^{20,21}\text{Ne}$ reaction rates and the applicability of the statistical model for nuclei with $A \lesssim 20$, [Phys. Rev. C](#) **96**, 045808 (2017).

[38] T. Rauscher, [Computer code EXP2RATE v2.1](#) (2025).

[39] T. Rauscher, P. Mohr, I. Dillmann, and R. Plag, Opportunities to constrain astrophysical reaction rates for the s-process via determination of the ground-state cross-sections, [The Astrophysical Journal](#) **738**, 143 (2011).

[40] R. H. Cyburt, A. M. Amthor, R. Ferguson, Z. Meisel, K. Smith, S. Warren, A. Heger, R. D. Hoffman, T. Rauscher, A. Sakharuk, H. Schatz, F.-K. Thielemann, and M. Wiescher, The JINA REACLIB Database: Its recent updates and impact on Type I X-ray Bursts, [Astrophys. J. Suppl. Ser.](#) **189**, 240 (2010), includes theory rates from T. Rauscher as part of REACLIB V1.0 release used in this work.

[41] C. Iliadis, [Nuclear Physics of Stars](#) (Wiley-VCH, Weinheim, 2007).